Pre-Exposure Embrittlement and Stress Corrosion Cracking of Magnesium Alloy AZ31B in Chloride Solutions

Mariano Kappes,[‡,,***] Mariano Iannuzzi,[***] and Ricardo M. Carranza[**]*

ABSTRACT

Stress corrosion cracking of the Mg-Al-Zn AZ31B (UNS M11311) alloy was studied in sodium chloride (NaCl) solutions at different potentials and NaCl concentrations using the slow strain rate technique. Results showed that stress-strain curves were similar despite changes in potential and chloride concentration. In addition, pre-exposure tests were performed in NaCl solutions at the open-circuit potential followed by immediate straining or straining after a dry-air exposure delay. The dependence of ductility with pre-exposure time, the reversibility of embrittlement, and the fracture surface of pre-exposed samples suggested that the AZ31B alloy was susceptible to internal hydrogen embrittlement. Stress corrosion cracking and the pre-exposure embrittlement of this alloy in NaCl environments are explained assuming that crack growth rate was controlled by hydrogen diffusion.

KEY WORDS: diffusion, hydrogen embrittlement, sodium chloride, stress corrosion cracking

INTRODUCTION

Given their high strength-to-density ratio, magnesium and magnesium alloys offer unique weight reduction opportunities in structural applications. However, Mg alloys are inheritably susceptible to stress corrosion cracking (SCC) in a variety of environments, including distilled water[1-5] and aqueous solutions of ubiquitous species like sodium chloride (NaCl)[1,6] or sulfates.[7] Current recommendations to avoid SCC of magnesium alloys suggest limiting design stresses to less than 50% of the yield strength (YS),[8-9] negatively impacting the attractiveness of those alloys for load-bearing applications.

Most investigations on SCC of Mg-Al alloys to date have been conducted in either high pH[7] or chromate-containing solutions,[10-20] which allow the formation of protective films, or in very mild environments such as deionized (DI) water.[2,4-5,21-22] Mg alloys are also prone to SCC in environments where they suffer active corrosion; e.g., SCC of the AZ31 (UNS M11311).[(1)] Mg-Al-Zn alloy in chloride solutions was reported by several authors,[6,23-26] where SCC proceeds alongside anodic dissolution.

It is now well known[27-28] that AZ31 suffers localized attack in chloride-containing solutions. Localized corrosion occurs by the expansion of dendrite-like features that eventually cover the entire surface. Localized corrosion starts at Mn-Al intermetallic particles, and proceeds without the formation of deep pits.[28] Once the entire surface is covered with dark corrosion products, the attack can be classified as uniform, with anodes that remain spatially mobile.[28] For pure magnesium with 50 ppm Fe corroded in NaCl solutions, it was shown, using cross-sectional analysis in the transmission electron microscope (TEM), that this dark corrosion zone consists of magnesium oxide (MgO) and hydroxide ($Mg[OH]_2$) on top of a MgO film,

Submitted for publication: October 22, 2013. Revised and accepted: January 21, 2014. Preprint available online: February 3, 2014, doi: http://dx.doi.org/10.5006/1172.

‡ Corresponding author. E-mail: marianokappes@hotmail.com.
* National Center for Education and Research on Corrosion and Materials Performance (NCERCAMP), The University of Akron, Akron (OH).
** Comisión Nacional de Energía Atómica, Instituto Sabato (UNSAM/CNEA), Argentina.
*** General Electric, Oil and Gas, Sandvika, Norway.

(1) UNS numbers are listed in *Metals and Alloys in the Unified Numbering System*, published by the Society of Automotive Engineers (SAE International) and cosponsored by ASTM International.

ISSN 0010-9312 (print), 1938-159X (online)
14/0000107/$5.00+$0.50/0

with Fe-rich particles embedded on the upper film.[29] This corroded zone was enriched in noble metal-rich particles, which, depending on alloy composition and impurity level, could include Fe, Ni, Mn, Cu, or even Al, and it catalyzes the hydrogen evolution reaction.[29]

Most cases of SCC involve materials in their passive state.[30] However, SCC of the AZ31 alloy in chloride-containing solutions[6,23-25] occurs alongside general corrosion. Contributions from anodic dissolution[23] and hydrogen embrittlement[6,23-25] were considered to explain the susceptibility of alloy AZ31 to SCC in chloride-containing solutions. Song, et al.,[6] observed a continuous decrease in tensile properties with pre-exposure time and absence of chlorides in the fracture surface. Song, et al.,[6] suggested this observation was evidence of internal hydrogen embrittlement in pre-exposed tests and that the same mechanism-controlled crack growth during SCC. However, a continuous decrease in mechanical properties with pre-exposure time is not enough evidence to sustain a hydrogen embrittlement mechanism. For instance, an anodic damage accumulation and stress concentration mechanism, such as that suggested by Kappatos, et al.,[24] might also justify this observation. Likewise, while an alloy might exhibit internal hydrogen embrittlement in a given environment, this does not mean that a hydrogen embrittlement-based process will control crack growth rate of that alloy during full immersion.[31]

Proposed anodic dissolution-based SCC mechanisms include the slip-dissolution model and the anodic-reaction-induced cleavage.[32] The slip-dissolution model requires the presence of passivating films.[32] Under localized strain, the passivating film might crack exposing bare metal that causes the crack to advance by dissolution, which then repassivates and the process can start over again.[32] The anodic-reaction-induced cleavage mechanism involves the formation of a thin oxide, nitride, chloride, or porous metallic film that with application of stress can fracture, inducing a brittle crack in the ductile substrate.[33]

The slip-dissolution mechanism can be discarded for AZ31 in chloride-containing solutions given that the alloy corrodes uniformly at steady state.[27-28] Song, et al.,[6] and Kappatos, et al.,[24] reported a continuous decrease in mechanical properties with increasing exposure time. It would be difficult to explain this pre-exposure effect based solely on models like the film-induced cleavage mechanism,[33] which rely on the formation of surface films. If anodic processes contribute to this pre-exposure effect, they have to be based on other processes such as a decrease in cross section or the formation of defects that act as stress concentrators.

Evidence of internal hydrogen embrittlement of Mg and Mg-Al alloys was discussed in various reviews.[9,34-36] Low hydrogen concentrations (i.e., between 16 ppm and 35 ppm) cause a decrease in impact properties due to grain boundary segregation,[37-38] whereas concentrations around 100 ppm or larger cause a decrease in tensile properties.[18] However, pre-exposure tests in chloride solutions, in all cases, show extensive anodic damage.[1,6,39] Tests on Mg and Mg alloy samples pre-corroded in chloride solutions conducted in air showed a decrease in ductility and ultimate tensile strength (UTS),[1,6,24] which was not as severe[1,6] as the one experienced by the sample stressed in situ. This decrease in ductility was explained in terms of a hydrogen embrittlement model[1,6] or an accumulated anodic damage model.[24] In the second model, it is believed that pits act as stress concentration sites, which decrease ductility.[24] However, cross sections of the so-called pits presented by the authors[24] show that they tend to grow faster in diameter than in depth, raising doubts about their ability to act as stress concentrators. In this regard, it is commonly accepted that to act as a stress concentration site the aspect ratio (i.e., the ratio between the pit opening and depth) has to be above 1:10.[40] In other systems, such as Mg-7.6 wt% Al in chloride-chromate mixtures,[18] pure Mg in basic sulfate solutions[7] and AZ80 (UNS M11800) Mg-Al-Zn alloy in chloride solutions,[1] the decrease in ductility and UTS could partly be reversed with a hydrogen desorption step. Those tests could resolve whether the decrease in ductility of AZ31 in chloride solutions during pre-exposure tests was due to hydrogen embrittlement[1,6] or irreversible anodic damage.[24]

The objective of this work was to determine if pre-exposure embrittlement of Mg alloy AZ31 is caused by an anodic-based process or internal hydrogen embrittlement. Additional tests were conducted to determine the relative importance of anodic dissolution vs. hydrogen embrittlement-based processes for SCC of AZ31 Mg alloy in chloride-containing solutions.

EXPERIMENTAL PROCEDURES

Electrochemical polarization tests were conducted using a conventional three-electrode cell. The electrolyte was 0.01 M NaCl at 30°C. Samples were abraded to 600 grit silicon carbide (SiC) paper and exposed to a 5,000 s open-circuit potential (OCP) delay just before starting the polarization experiment. Potential was measured with a saturated calomel electrode (SCE), and a graphite bar was used as a counter electrode. Anodic and cathodic curves were obtained in separate experiments. The potential was scanned from OCP at a rate of 0.166 mV/s. All tests were conducted in triplicate to address reproducibility.

Electrochemical impedance spectroscopy (EIS) tests were conducted to estimate the polarization resistance (R_P) at different chloride concentrations. Tests were conducted after 1 day of OCP exposure, to estimate steady-state corrosion rates. Frequency

TABLE 1
Nominal Chemical Composition (in wt%) of the AZ31B Alloy

Al	Zn	Mn	Si	Cu	Ca	Fe	Ni	Mg
2.5 to 3.5	0.7 to 1.3	>0.2	<0.05	<0.05	<0.04	0.005	0.005	Balance

was scanned from 100 kHz down to 10 mHz, with 7 points/decade and an alternating current (AC) root mean square (rms) amplitude of 10 mV_{rms}. EIS results were fitted with a simplified Randles circuit modified[41] with a constant phase element. When an inductive loop was observed at low frequency, the equivalent circuit recently proposed by King, et al.,[42] was used. This equivalent circuit contains two capacitors, one inductor, and four resistances, including the solution resistance. The reader is referred to the original paper[42] for details of the circuit construction, physical significance of each element, and equation for obtaining R_P from the fitting parameters.

Slow strain rate tests (SSRT) were conducted on round tension test specimens, with a gauge diameter of 4 mm and a gauge length of 25 mm. Samples were machined from a 6.5 mm extruded AZ31B bar (UNS M11311). The nominal composition of this alloy is presented in Table 1. The mechanical properties, quoted in the materials certificate of conformance, are YS = 188 MPa, UTS = 262 MPa, and ductility = 22% (measured on a 50.8 mm bar). The microstructure of this commercial alloy was studied elsewhere, and it is expected to consist of Mg grains with Mn-Al intermetallic inclusions.[27,43] To minimize hydrogen absorption from humid air,[44] samples were kept in a desiccator until testing. At this point, samples were manually ground with 600 grit SiC paper and rinsed with 200-proof ethanol. Samples were then placed in a three-electrode SCC cell and strained at a rate of 4×10^{-6} s^{-1}. The potential of the working electrode was measured with a SCE fitted in a Luggin capillary. A Pt counter electrode was used for tests conducted at a fixed applied potential. The solution was re-circulated at a rate of 300 mL/min from a 5 L reservoir kept at 30°C, minimizing solution composition variations (particularly pH) during testing (Figure 1).[21] After the test, samples were examined using scanning electron microscopy (SEM).

SSRT tests were conducted under a different set of variables. For each combination of variables, tests were conducted in duplicate at least. Most tests were performed in a 0.01 M NaCl solution. Some tests were performed in 0.1 M NaCl and 0.001 M NaCl to explore the effect of chloride concentration on SCC behavior, as indicated. The effect of potential was investigated by conducting tests at OCP in 0.01 M NaCl, at –1.35 V_{SCE}, an anodic potential beyond the breakdown potential measured in polarization curves, and at –1.9 V_{SCE}, a cathodic potential where hydrogen evolution is increased at the expense of reduced anodic damage.[45] A test in air was also conducted as control.

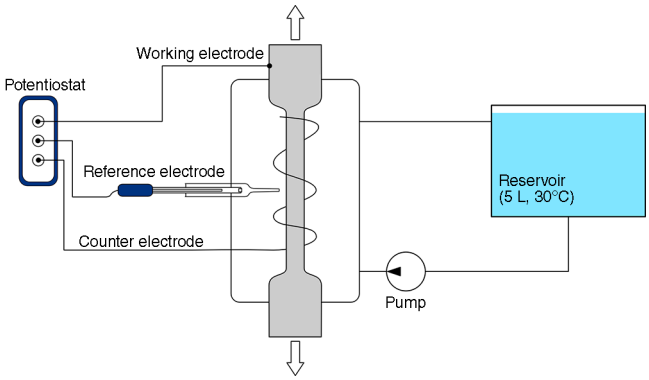

FIGURE 1. *Experimental setup for SSRT.*

To investigate the pre-exposure effect, unloaded samples were exposed at OCP for 1 day in 0.1 M NaCl or 0.01 M NaCl, thus potentially allowing hydrogen to be charged into the metal or anodic damage to be accumulated. After removing the samples from the environment, they were rinsed with DI water and 200-proof ethanol and immediately tested in laboratory air. For the 0.01 M NaCl solution, this test was repeated for 4 days' pre-exposure to check the effect of increased exposure time. To explore whether the decrease in ductility of a pre-exposed sample found here and reported by others[6,24] was due to irreversible anodic damage or to reversible hydrogen charging, a new set of samples was first pre-exposed at OCP for 24 h to a 0.1 M NaCl solution and subsequently left in a desiccators for 13 days or 28 days to allow desorption of any absorbed hydrogen.

RESULTS

Figure 2 shows anodic and cathodic polarization curves of AZ31B in 0.01 M NaCl after 5,000 s of OCP exposure. Dotted lines indicate the selected potential values for SSRT. A breakdown potential, E_b, was observed at –1.43±0.03 V_{SCE}, indicated by an arrow. This value is close to the one reported by Przondziono, et al.[46] Breakdown of the protective film manifested itself as expanding dark corroded regions that eventually covered the entire surface of the sample. Other authors[28] studying the same alloy determined that this dark corroded region consisted of a zone enriched with Al-Mn particles, which caused cathodic activation and enhanced hydrogen evolution.[29]

The in-air YS of AZ31B was 158 MPa, the UTS was 273 MPa, and the elongation to failure was 20.4%, Figure 3, which is close to typical values reported for extruded products.[47] Results are also in

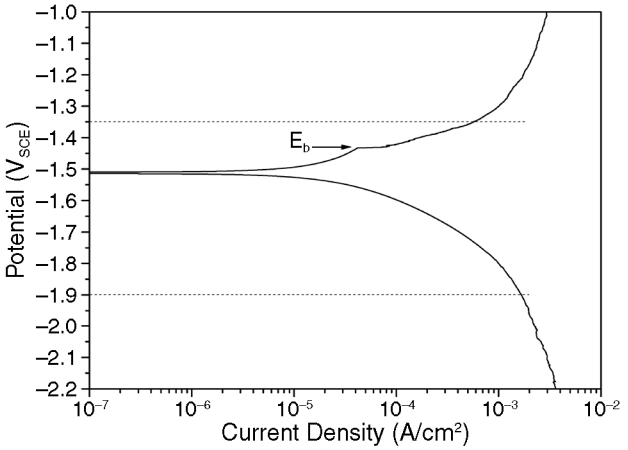

FIGURE 2. *Polarization curves of AZ31B Mg alloy in 0.01 M NaCl. Dotted lines show the values of potential where SSRT were conducted, and the arrow points the E_b.*

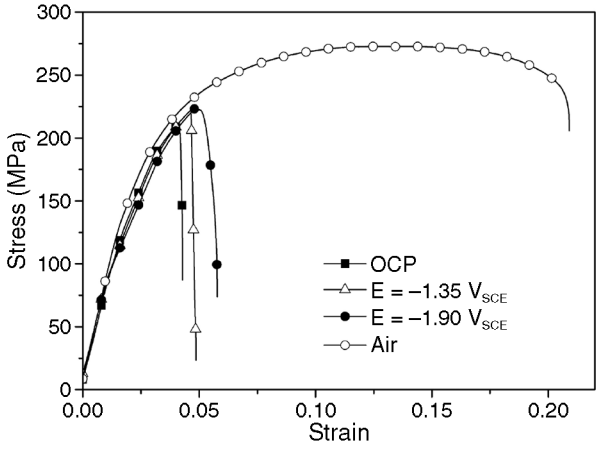

FIGURE 3. *SSRT of AZ31B Mg alloys immersed in 0.01 M NaCl solution at 30°C showing the effect of potential. The curve in air is included for comparison.*

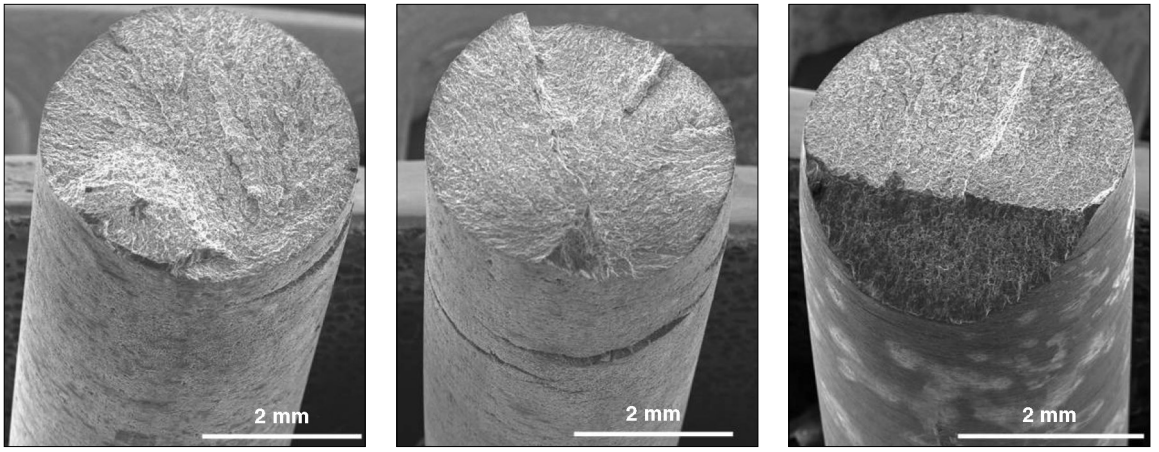

FIGURE 4. *Secondary electron images of AZ31B SSRT samples tested under full immersion in 0.01 M NaCl: (a) at the OCP, (b) at E = –1.35 V_{SCE}, and (c) E = –1.90 V_{SCE}.*

reasonable agreement with the mechanical properties quoted in the material's certificate for the alloy, as presented above. On the other hand, samples under full immersion showed a significant reduction in strain to failure at all potential values, Figure 3. Failure of the samples occurred under stable crack propagation, during which the load decreased continuously until the point where the remaining ligament was cracked. Cracking occurred at low loads, typically below 100 MPa. SEM examination revealed that cracks were transgranular. In addition, for tests performed at OCP or at an anodic potential, secondary cracks were observed along the gauge length, Figure 4. Fracture of the tensile samples had, in some cases, a stepped appearance as a result of the joining of transgranular cracks that grew separately, Figure 4(b), for the sample tested at the anodic potential.

The surface of samples exposed at OCP and at anodic potential exhibited uniform attack after being removed from solution, with no tendency to pitting. On the other hand, the sample exposed at a cathodic potential was covered with a gray film, Figure 4(c). It is likely that this film was $Mg(OH)_2$, which can be formed even at cathodic potentials[7,48] due to water decomposition of magnesium hydrides.[48] Other authors[7] reported that this film remained intact during preexposure in a sulfate solution under a cathodic potential, preventing hydrogen absorption and internal hydrogen embrittlement. In DI water[21] and chloride-containing solutions,[23] the film could be ruptured during straining, making hydrogen absorption possible and causing SCC susceptibility at cathodic potentials.

Figure 5 shows the effect of chloride concentration on the stress-strain curves. Maximum stress and maximum elongation increased slightly with a decrease in chloride concentration. These results are in accord with those previously shown by Song, et al.,[6] where both ductility and UTS of AZ31 in chloride-

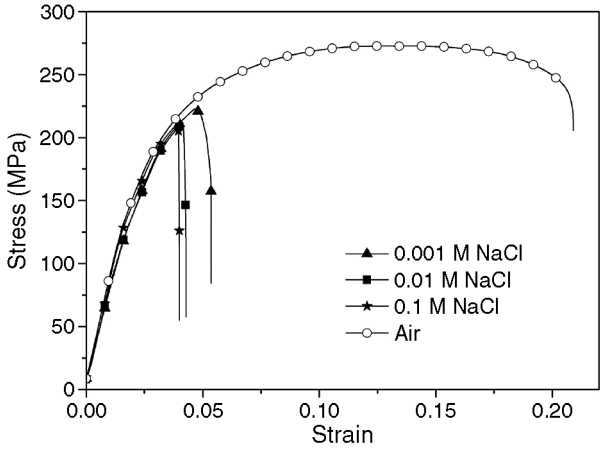

FIGURE 5. *SSRT of AZ31B Mg alloys performed at OCP and 30°C in solutions containing different NaCl concentrations. The curve in air is included for comparison.*

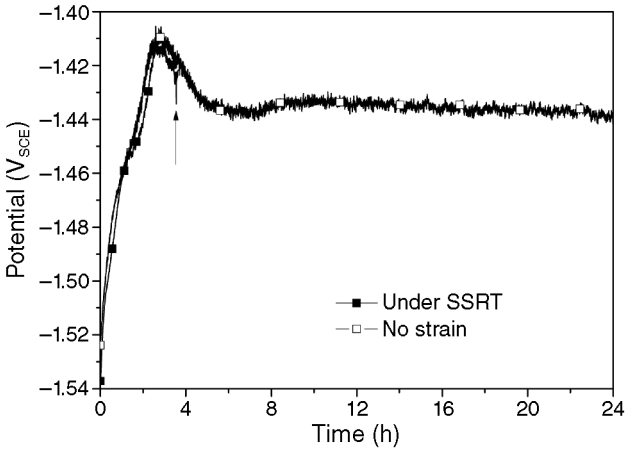

FIGURE 6. *Corrosion potential vs. time curves for AZ31B Mg alloy samples exposed to 0.01 M NaCl under a SSRT and under no load. The arrow indicates the end-point of the SSRT test due to sample failure.*

containing environments were not a strong function of chloride concentration. Fracture surfaces had a similar appearance at all chloride levels, with transgranular cracks and secondary cracks similar to those presented in Figure 4(a). Breakdown of the protective film was observed in all cases, evidenced by the appearance of dark spots on the originally shiny surface. A maximum in the corrosion potential vs. time curve was observed for the solution containing 0.01 M NaCl, Figure 6, in accordance with Williams, et al.[28] The OCP at steady state was close to the breakdown potential value measured in the polarization tests. The stressed samples failed at potentials above the breakdown potential, but just before reaching steady state. The OCP measured during SSRT was similar to the potential measured with no strain, suggesting that stress had little effect on the breakdown of the film spontaneously formed in air prior to exposure.

Figure 7 shows complex plots obtained for AZ31B magnesium alloy at three different chloride concentrations, and the fitting lines of the equivalent circuit selected to estimate a R_P value. In the impedance curves obtained in 0.1 M NaCl and 0.01 M NaCl, an inductive response was observed at low frequencies. Those curves were fitted with the equivalent circuit proposed by King, et al.[42] R_P was obtained from the value of the real impedance taken at the low-frequency end of the spectra (Figure 7). The curve obtained at 0.001 M NaCl presented some scatter at low frequencies, but a single time constant-type response was apparent. Therefore, this curve was fitted with a simplified Randles circuit modified with a constant phase element. The focus of those measurements was to estimate R_P, which is inversely related to the corrosion rate.[42] For solutions containing 0.001 M NaCl, 0.01 M NaCl, and 0.1 M NaCl, the calculated R_P values were 4,800, 825, and 84 $\Omega \cdot cm^2$, respectively. It is important to highlight that the R_P value obtained in 0.001 M NaCl could be in error by a factor of 2 or more if it exhibited an in-

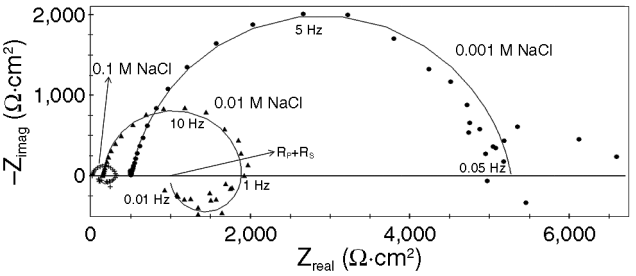

FIGURE 7. *Complex plots, showing the effect of chloride concentration on the EIS response of AZ31B in 0.001, 0.01, and 0.1 M NaCl at 30°C. For the curves obtained in 0.1 M NaCl and 0.01 M NaCl with an inductive response at low frequency, the value of $R_P + R_S$ can be obtained graphically as shown for the curve in 0.01 M NaCl.[41] Symbols: experimental results. Lines: equivalent circuit fitting.*

ductive response at lower frequency as observed in the more concentrated solutions. Despite this potential source of error, these results are in good agreement with the increasing corrosion rate as a function of chloride concentration presented by other authors for this alloy.[28]

Figure 8 shows the results of SSRT aimed at studying the mechanism of pre-exposure embrittlement of AZ31 alloy exposed to chloride-containing solutions. After 24 h OCP pre-exposure in a 0.01 M NaCl solution (test condition 1), a sample strained in air showed a maximum stress similar to the unexposed control and an elongation to failure intermediate between full immersion and in air. Part of this elongation could be recovered by a 13 day exposure to dry air inside a desiccator (test condition 2), suggesting that there was a net, reversible contribution from absorbed mobile hydrogen. This partial recovery of ductility is in accordance with results presented by

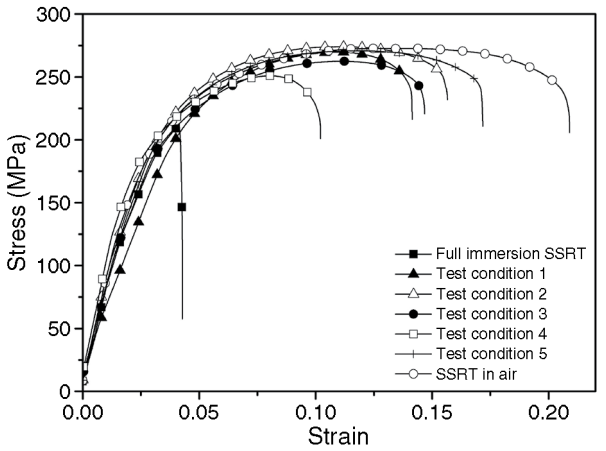

FIGURE 8. *SSRT of AZ31B Mg alloys performed under different conditions: full immersion at the OCP in 0.01 M NaCl at 30°C (■), tested in air immediately after 24 h OCP exposure to 0.01 M NaCl at 30°C (test condition 1, ▲), tested in air after 24 h OCP exposure to 0.01 M NaCl at 30°C followed by a 13 day exposure to dry air (test condition 2, △), tested in air immediately after 24 h OCP exposure to 0.1 M NaCl at 30°C (test condition 3, ●), tested in air immediately after 96 h OCP exposure to 0.01 M NaCl at 30°C (test condition 4, □), tested in air after 24 h OCP exposure to 0.01 M NaCl at 30°C followed by a 28 day exposure to dry air (test condition 5, +). The curve in air of an unexposed specimen is included for comparison (○).*

other authors for Mg-Al 7.6 wt% in chloride-chromate mixtures,[18] pure Mg in basic sulfate solutions,[7] and AZ80 Mg-Al-Zn alloy in chloride solutions[1]. Reversibility of embrittlement due to hydrogen desorption after a hydrogen charging step, as reported in this work, has also been observed in other systems, such as commercially pure Ti,[49] a Ti-13V-11Cr-3Al alloy,[50] 7000 series aluminum alloys,[31,51-57] and steels.[55,58-64] In all cases, this observation was an indication that absorbed mobile hydrogen contributed to the observed decrease in mechanical properties in pre-exposed tests.

A set of experiments was conducted to investigate further the cause of the ductility loss observed during pre-exposure tests. A tensile sample was immersed in 0.1 M NaCl for 24 h, and then strained in air (test condition 3). Although the corrosion rate was about an order of magnitude larger in 0.1 M NaCl than in 0.001 M NaCl, Figure 7, the loss in ductility was similar to the one measured for the sample pre-exposed to 0.01 M NaCl for the same time period (test condition 1). This finding suggests that a decrease in cross section caused by corrosion was not responsible for the decrease in ductility observed in pre-exposed tests.

Another tensile sample was immersed for 96 h in 0.01 M NaCl (test condition 4). This resulted in decreased ductility and maximum stress with respect to the samples pre-exposed for 24 h. The observed dependence between ductility and UTS with pre-exposure time is in accordance with results by Song, et al.,[6] and Kappatos, et al.,[24] for the same Mg alloy and by Chakrapani and Pugh[18] for a Mg-Al alloy. Other systems such as 7000 series aluminum alloys pre-exposed to water vapor,[53,57,65] seawater,[51] or tap water,[31] and carbon steels pre-exposed to sour environments[66] show this behavior as well, which is a known consequence of hydrogen embrittlement.

Finally, in this system (test condition 2) and in other Mg alloy-environment systems,[1,7,18] it was found that ductility of a corroded sample can be partly recovered with exposure to an environment with low hydrogen activity. In this case, it is plausible that ductility values did not reach that of the unexposed sample due to either residual hydrogen or anodic damage. Another sample was pre-exposed in 0.01 M NaCl for 24 h, and then left in dry air for 28 days (test condition 5), doubling the time of the samples of test condition 2. Test condition 5, with the additional drying time, resulted in approximately a 10% increment in ductility compared to test condition 1 (Figure 8).

SEM examination of those samples supported the idea of a reversible contribution from hydrogen (Figure 9). A much higher density of secondary cracks was observed on the lateral surfaces of specimens that were immediately stressed after OCP exposure (test conditions 1 and 4) than on those specimens that were exposed to dry air prior to being strained (test conditions 2 and 5), suggesting those cracks were a manifestation of hydrogen embrittlement.

In accordance with these observations, crack surfaces of the pre-exposed specimens that were immediately strained showed a central ductile region surrounded by an annular region that failed by cleavage (Figure 10). The dry air exposure was effective in eliminating this annular, cleavage region. The entire crack surface of those samples exhibited a ductile fracture (Figure 11). This suggests that the material in the annular region failed by cleavage as a result of the combination of stress and hydrogen.

The width of this annular, hydrogen-embrittled region was a function of OCP pre-exposure time (Figure 10). The width of the hydrogen-embrittled region of a sample pre-exposed for 24 h was around 375 μm. A fourfold increase in pre-exposure time resulted in an annular, embrittled region with a width of 720 μm, which is about double the width obtained in the shorter OCP exposure. This relationship suggests that embrittlement was controlled by hydrogen diffusion. Holroyd and Hardie[51] used the depth of embrittlement, x, to calculate the hydrogen diffusion coefficient for aluminum alloy (AA)7049-T651 (UNS A97049) pre-exposed in seawater. In that case, x should scale as:

$$x \sim 4Dt \quad (1)$$

where D is the diffusion coefficient and t the immersion time. Based on the results shown above, a rough estimate of D gives 10^{-9} cm^2/s.

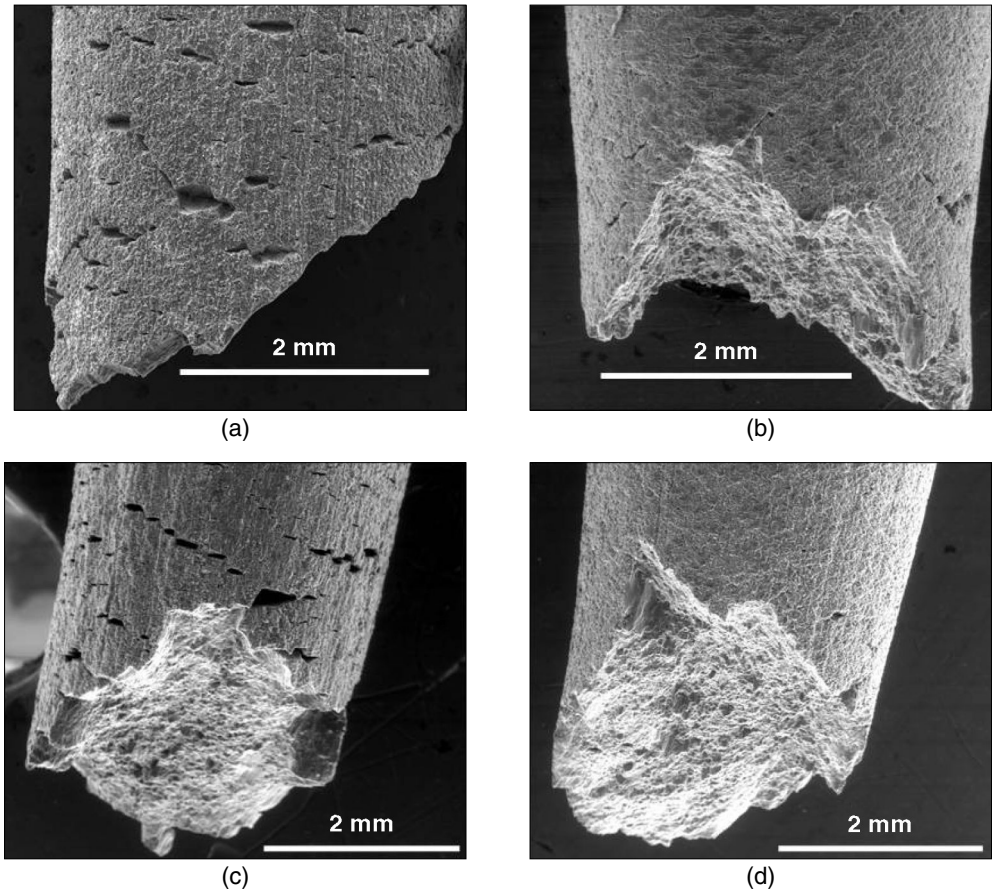

FIGURE 9. *Secondary electron images of AZ31B SSRT samples tested in air immediately after 24 h OCP exposure to 0.01 M NaCl at 30°C, test condition 1, (a), tested in air after 24 h OCP exposure to 0.01 M NaCl at 30°C followed by a 13 day exposure to dry air, test condition 2 (b), tested in air immediately after 96 h OCP exposure to 0.01 M NaCl at 30°C, test condition 4, (c), and tested in air after 24 h OCP exposure to 0.01 M NaCl at 30°C followed by a 28 day exposure to dry air, test condition 5 (d).*

DISCUSSION

The reversible, pre-exposure embrittlement effect (test conditions 1, 3, and 4 vs. test conditions 2 and 5) observed in this work suggest that this alloy was susceptible to internal hydrogen embrittlement.[55] Fractography results, where the width of the annular brittle region doubled with a fourfold increase in pre-exposure time, suggested that pre-exposure embrittlement was controlled by hydrogen diffusion. This was used to estimate a value for the hydrogen diffusion coefficient of 10^{-9} cm^2/s. There is considerable scatter[35] on the value of the hydrogen diffusion coefficient at room temperature estimated by different authors for Mg and its alloys. Makar, et al.,[10] and Dietzel, et al.,[22] estimated values of the hydrogen diffusion coefficient indirectly from mechanical tests, similar to the approach used herein. Values of 2×10^{-9} cm^2/s were obtained for a Mg-Al[10] and a Mg-Al-Zn[22] alloy. Knotek, et al.,[67] using the Devanathan and Stachurski approach,[68] obtained a value of 6.7×10^{-9} cm^2/s for pure Mg. Spatz, et al.,[69] reported a value of 1.1×10^{-16} cm^2/s based on the growth kinetics of magnesium hydride (MgH_2), for pure Mg near room temperature. Finally, Atrens, et al.,[70] extrapolated high-temperature results of hydrogen diffusion in pure Mg,[71-72] obtaining a value of 10^{-5} cm^2/s.[70] The approach we adopted in this work is indirect and relies on the interaction between stress and hydrogen to give a brittle failure. There are several sources of error, including the formation of corrosion films that might slow down hydrogen absorption and the propagation of brittle failure beyond the zone saturated by hydrogen. Despite this, the value estimated falls within the scatter band reported in the literature.

Pre-corroded tensile samples of AZ31B Mg alloy showed a decrease in ductility and UTS that was a function of the pre-exposure time (test conditions 1 and 4), similar to results presented for this same system by Song, et al.,[6] and Kappatos, et al.[24] Based on evidence presented here, embrittlement was likely the result of increased time for hydrogen diffusion. Decrease in cross section and stress concentration by defects,[24] which could also explain this dependence,

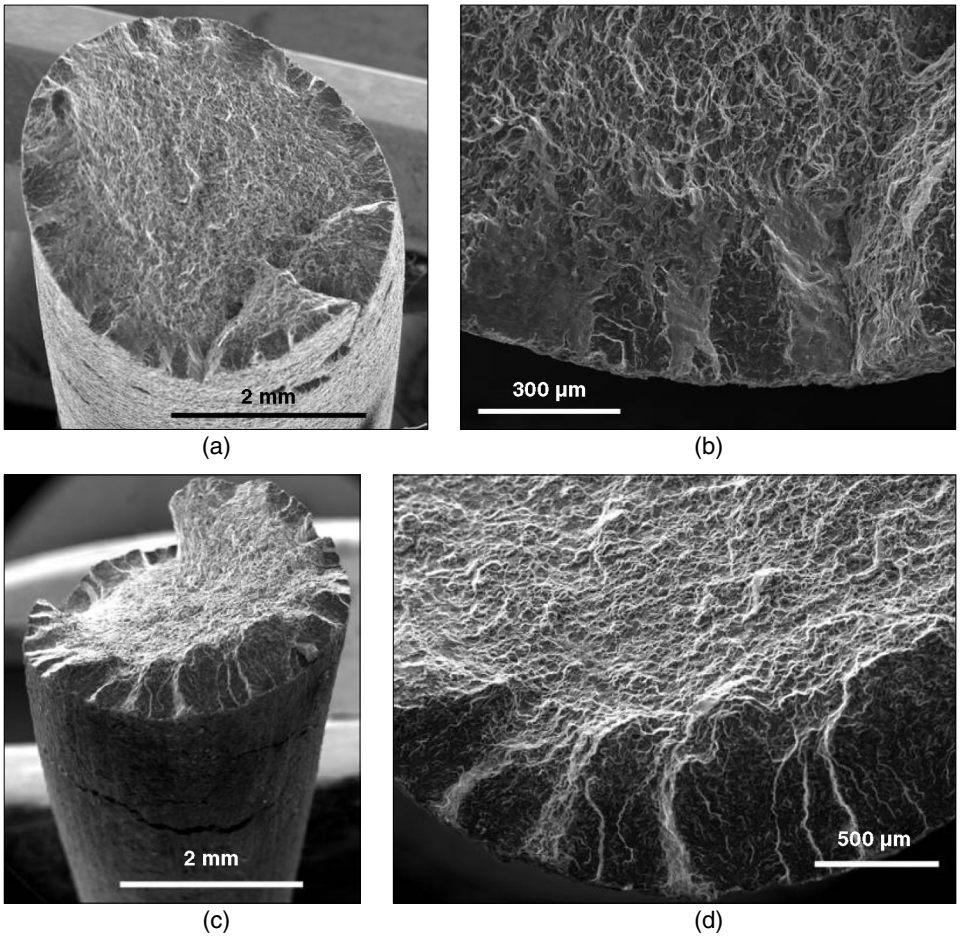

FIGURE 10. *Secondary electron images of AZ31B SSRT samples tested in air immediately after an OCP exposure to 0.01 M NaCl at 30°C. Pre-exposure time was 24 h, test condition 1 (a) and (b) and 96 h, test condition 4 (c) and (d).*

were not controlling processes here because the loss of ductility was partly recovered by exposure to dry air (test conditions 2 and 5). Furthermore, deep pits are not expected to form during corrosion of this alloy in chloride solutions.[28] Fractographies were consistent with the hypothesis of hydrogen embrittlement: for test conditions 1 and 4, Figure 10 shows secondary cracks and a central ductile region, surrounded by an annular region that failed by cleavage and with a width that doubled after increasing the exposure time by four times, in accordance with Equation (1). For test conditions 2 and 5, Figure 11, a fully ductile fracture was observed with no secondary cracks. Finally, from the R_P values obtained in 0.1 M NaCl and 0.01 M NaCl, the corrosion rate is expected to increase an order of magnitude with the tenfold increase in chloride concentration. Despite this, pre-exposing a tensile sample for 1 day in those environments resulted in a similar decrease in ductility and maximum tensile strength, suggesting anodic processes are not rate-limiting.

Ductility of the AZ31B samples exhibited dependence with dry air exposure time. Even after 13 days of dry air exposure (test condition 2), ductility was not completely recovered. The greater ductility measured after increasing the dry air exposure time, test condition 5, is an indication of the sluggish diffusion of hydrogen. Hydrogen in this case would also have to diffuse through corrosion products, containing $Mg(OH)_2$, which can hinder hydrogen transport outbound from the sample.[35] Furthermore, the presence of defects such as dislocations, grain boundaries, and particles could act as traps slowing down hydrogen desorption. Other authors[18] performed vacuum heat treatments at temperatures above the magnesium hydride decomposition temperature to accelerate the hydrogen desorption process; however, this was not attempted here because grain growth of AZ31B alloy was reported at temperatures as low as 200°C.[73]

While the results discussed so far suggest that Mg alloy AZ31B exhibits internal hydrogen embrittlement when exposed to NaCl solutions, the contribution from a hydrogen-assisted mechanism during SCC has yet to be discussed. It was found that, in chloride-containing solutions, potential and chloride concentration did not have a great effect on the SCC susceptibility of alloy AZ31B measured by SSRT at a strain rate of 4×10^{-6} s^{-1}. SCC susceptibility was simi-

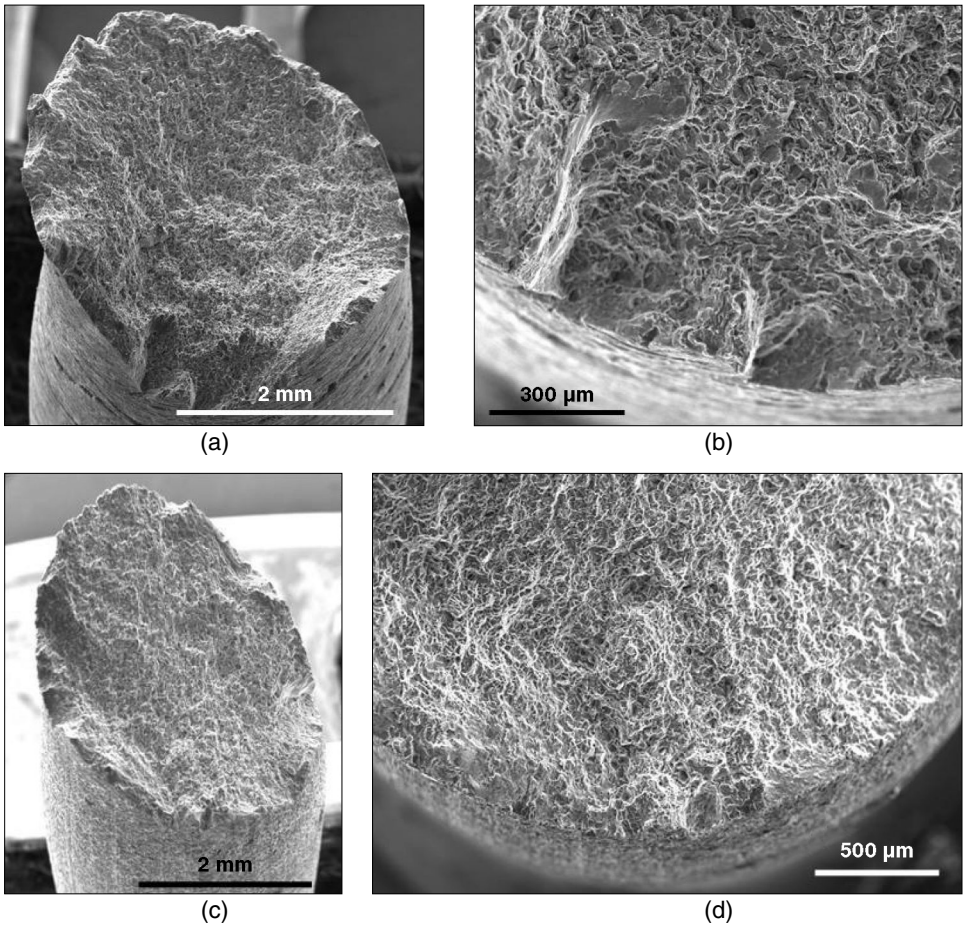

FIGURE 11. *Secondary electron images of AZ31B SSRT samples tested in air after 24 h OCP exposure to 0.01 M NaCl at 30°C, followed by dry air exposure. Dry air exposure time was 13 days, test condition 2 (a) and (b), and 28 days, test condition 5 (c) and (d).*

lar at a cathodic potential, where anodic damage is reduced,[45] at OCP, and at an anodic potential above the E_b, suggesting that anodic processes were not rate-controlling.[74] Also, despite the strong dependence between corrosion rates and chloride concentration reported for this alloy herein and elsewhere,[28] SCC susceptibility was similar at all chloride levels.

A model based on hydrogen-assisted cracking could explain many of the observed facts, including the SCC susceptibility at cathodic potentials. However, despite that Mg hydrogen evolution increases with anodic[75-76] and cathodic[29,75] potentials and with chloride concentration,[28] SCC susceptibility did not show a strong dependence with those variables. One possibility could be that due to the sluggish hydrogen[35] diffusion, crack advance was controlled by diffusion of hydrogen to the crack tip zone. This mechanism, though not rigorously validated with the data presented here, could explain the independence of SCC intensity with chloride concentration and potential.

Results of crack propagation rate performed at different temperatures presented elsewhere determined that for a WE54 (UNS M18410) Mg[77] alloy in distilled water, the crack propagation rate had an activation energy near 50 kJ/mol. There is significant dispersion on the reported activation energy values for the hydrogen diffusion coefficient, which ranges from 40 kJ/mol[78] to 24 kJ/mol.[71] The first value seems more reasonable because, in that case, the activation energy would be close to values reported for other hexagonal closed-packed metals (hcp), like α-Ti[79] and Zr.[80] Vogt and Speidel[77] concluded that due to the similarities in activation energy for hydrogen diffusion and crack propagation rate, it is possible that this process is the rate-controlling step during SCC. Despite the differences in alloy and environment composition, those results and the ones reported herein, suggest that hydrogen diffusion is the rate-determining step during SCC of magnesium alloys.

Despite the fact that OCP pre-exposure caused hydrogen embrittlement, pre-exposed tests could not mimic ductility loss and fracture appearance obtained in full immersion tests. Even after 4 days of pre-exposure to OCP, the samples had a central ductile region, unlike samples tested in the environ-

ment where a cleavage fracture propagated covering almost the entire area of the specimen (Figure 4). This suggests that the time and sample diameter selected were insufficient for hydrogen saturation during OCP pre-exposure. It is likely that during tests performed under immersion, hydrogen was provided by hydrogen evolution reaction in the crack tip region. Tests under full immersion had a duration on the order of 12,500 s. Assuming cracks grew about 2 mm during this time, Figure 4, this gives an average crack growth rate, v, of 1.6×10^{-5} cm/s. Using the value of D estimated in this work, the D/v ratio was 6×10^{-5} cm. This coefficient is more than three orders of magnitude larger than the minimum value required to have a hydrogen atmosphere ahead of the moving crack,[81] suggesting hydrogen diffusion control is a possible mechanism. Furthermore, in the SCC tests under full immersion, hydrogen is expected to be charged into the sample concomitant with plastic deformation. This can result in enhanced transport by hydrogen atmospheres around mobile dislocations.[56]

CONCLUSIONS

SCC of the AZ31B Mg-Al-Zn alloy in chloride-containing solutions was studied under different chloride concentrations and potentials using the SSRT technique. Based on the evidence presented herein, the following conclusions were drawn:

❖ SCC susceptibility was not a strong function of chloride concentration or potential, despite the dependence of the anodic dissolution reaction on those variables.

❖ Potential measurements and visual observation during SCC testing indicated that cracks propagated alongside localized attack above the breakdown potential, which eventually propagated, covering the entire sample.

❖ The reversible, pre-exposure embrittlement effect observed in this system suggested that the alloy suffered internal hydrogen embrittlement.

❖ Ductility decreased with an increase in pre-exposure time and could be partially recovered with dry-air exposure. The diameter of the brittle, annular zone in the fractography of samples pre-exposed and then immediately strained, doubled with a fourfold increase in time. These observations suggest that pre-exposure embrittlement was controlled by hydrogen diffusion.

❖ Another manifestation of internal hydrogen embrittlement in this system was the presence of secondary cracks on the lateral surface of the tensile specimen, which were observed in specimens immediately strained but not on those that were strained after the dry air hydrogen desorption step.

REFERENCES

1. M. Bobby Kannan, W. Dietzel, *Mater. Des.* 42 (2012): p. 321-326.
2. N. Winzer, A. Atrens, W. Dietzel, V.S. Raja, G. Song, K.U. Kainer, *Mater. Sci. Eng. A* 488 (2008): p. 339-351.
3. N. Winzer, A. Atrens, W. Dietzel, G. Song, K.U. Kainer, *Mater. Sci. Eng. A* 472 (2008): p. 97-106.
4. N. Winzer, A. Atrens, W. Dietzel, *Adv. Eng. Mater.* 10 (2008): p. 453-458.
5. N. Winzer, A. Atrens, W. Dietzel, G. Song, K.U. Kainer, *Metall. Mater. Trans. A* 39 (2008): p. 1157-1173.
6. R.G. Song, C. Blawert, W. Dietzel, A. Atrens, *Mater. Sci. Eng. A* 399 (2005): p. 308-317.
7. R.S. Stampella, R.P.M. Procter, V. Ashworth, *Corros. Sci.* 24 (1984): p. 325-341.
8. E. Ghali, "Magnesium and Magnesioum Alloys," in *Uhlig's Corrosion Handbook*, 3rd ed., ed. R.W. Revie (Hoboken, NJ: John Wiley & Sons, 2000), p. 809-836.
9. N. Winzer, A. Atrens, G. Song, E. Ghali, W. Dietzel, K.U. Kainer, N. Hort, C. Blawert, *Adv. Eng. Mater.* 7 (2005): p. 659-693.
10. G.L. Makar, J. Kruger, K. Sieradzki, *Corros. Sci.* 34 (1993): p. 1311-1342.
11. R.H. Jones, J.S. Vetrano, C.F. Windisch, *Corrosion* 60 (2004): p. 1144-1154.
12. L. Fairman, H.J. Bray, *Corros. Sci.* 11 (1971): p. 533-541.
13. L. Fairman, H.J. Bray, *Br. Corros. J.* 6 (1971): p. 170-174.
14. L. Fairman, J.M. West, *Corros. Sci.* 5 (1965): p. 711-716.
15. K. Ebtehaj, D. Hardie, R.N. Parkins, *Corros. Sci.* 28 (1988): p. 811-829.
16. E. Meletis, R. Hochman, *Corrosion* 40 (1984): p. 39-45.
17. S.P. Lynch, P. Trevena, *Corrosion* 44 (1988): p. 113-124.
18. D.G. Chakrapani, E.N. Pugh, *Metall. Trans. A* 7 (1976): p. 173-178.
19. D.G. Chakrapani, E.N. Pugh, *Metall. Trans. A* 6 (1975): p. 1155-1163.
20. W.R. Wearmouth, G.P. Dean, R.N. Parkins, *Corrosion* 29 (1973): p. 251-258.
21. M. Bobby Kannan, W. Dietzel, R.K.S. Raman, P. Lyon, *Scr. Mater.* 57 (2007): p. 579-581.
22. W. Dietzel, M. Pfuff, N. Winzer, *Eng. Fract. Mech.* 77 (2010): p. 257-263.
23. Y. Uematsu, T. Kakiuchi, M. Nakajima, *Mater. Sci. Eng. A* 531 (2012): p. 171-177.
24. V. Kappatos, A.N. Chamos, S.G. Pantelakis, *Mater. Des.* 31 (2010): p. 336-342.
25. S. Kuramoto, I. Araki, M. Kanno, *J. Japan Inst. Light Met.* 51 (2001): p. 397-402.
26. L.C. Tsao, *Int. J. Mater. Res.* 101 (2010): p. 1166-1171.
27. M.C. Merino, A. Pardo, R. Arrabal, S. Merino, P. Casajús, M. Mohedano, *Corros. Sci.* 52 (2010): p. 1696-1704.
28. G. Williams, H. ap Llwyd Dafydd, R. Grace, *Electrochim. Acta* 109 (2013): p. 489-501.
29. M. Taheri, J.R. Kish, N. Birbilis, M. Danaie, E.A. McNally, J.R. McDermid, *Electrochim. Acta* 116, 10 (January) (2014): p. 396-403.
30. R.W. Staehle, *Mater. Sci. Eng.* 25 (1976): p. 207-215.
31. D. Hardie, N. Holroyd, R. Parkins, *Met. Sci.* 13 (1979): p. 603-610.
32. A. Turnbull, *Corros. Sci.* 34 (1993): p. 921-960.
33. K. Sieradzki, R.C. Newman, *J. Phys. Chem. Solids* 48 (1987): p. 1101-1113.
34. G.L. Makar, J. Kruger, *Int. Mater. Rev.* 38 (1993): p. 138-153.
35. M. Kappes, M. Iannuzzi, R.M. Carranza, *J. Electrochem. Soc.* 160 (2013): p. C168-C178.
36. D. Hardie, in *Environment-Induced Cracking of Metals*, eds. R.P. Gangloff, M.B. Ives (Houston, TX: NACE International, 1990), p. 347-361.
37. Y. Chino, D. Nishihara, T. Ueda, M. Mabuchi, *Mater. Trans.* 52 (2011): p. 1123-1126.
38. M. Yuasa, D. Nishihara, M. Mabuchi, Y. Chino, *J. Phys. Condens. Matter* 24 (2012): p. 1-9.
39. M. Bobby Kannan, W. Dietzel, C. Blawert, A. Atrens, P. Lyon, *Mater. Sci. Eng. A* 480 (2008): p. 529-539.
40. R.H. Jones, "Stress Corrosion Cracking," in *ASM Handbook: Vol. 13A: Corrosion: Fundamentals, Testing, and Protection*, eds. S.D. Cramer, B.S. Coving, Jr. (Materials Park, OH: ASM International, 2003), p. 346-366.
41. R. Cottis, S. Turgoose, *Corrosion Testing Made Easy: Impedance and Noise Analysis*, ed. B.C. Syrett (Houston, TX: NACE International, 1999).
42. A.D. King, N. Birbilis, J.R. Scully, *Electrochim. Acta* 121, 1 (March) (2014): p. 394-406.
43. A. Pardo, M.C. Merino, A.E. Coy, F. Viejo, R. Arrabal, S. Feliú, Jr., *Electrochim. Acta* 53 (2008): p. 7890-7902.
44. G.I. Morozova, *Met. Sci. Heat Treat.* 50 (2008): p. 100-104.

45. D. Najjar, T. Magnin, T.J. Warner, *Mater. Sci. Eng. A* 238 (1997): p. 293-302.
46. J. Przondziono, W. Walke, E. Hadasik, B. Jasinski, *Acta Metall. Slovaca* 16 (2010): p. 254-260.
47. M. Gupta, N.M.L. Sharon, *Magnesium, Magnesium Alloys, Magnesium Composites* (Hoboken, NJ: John Wiley & Sons, 2011).
48. G.G. Perrault, *Electroanal. Chem. Interfacial Electrochem.* 27 (1970): p. 47-58.
49. K. Ebtehaj, D. Hardie, R.N. Parkins, *Corros. Sci.* 25 (1985): p. 415-429.
50. R.W. Lycett, J.C. Scully, *Corros. Sci.* 19 (1979): p. 799-817.
51. N. Holroyd, D. Hardie, *Corros. Sci.* 2 (1981): p. 129-144.
52. R.E. Ricker, D.J. Duquette, *Metall. Trans. A* 19 (1988): p. 1775-1783.
53. G. Scamans, R. Alani, P. Swann, *Corros. Sci.* 16 (1976): p. 443-459.
54. R.J. Gest, A.R. Troiano, *Corrosion* 30 (1974): p. 274-279.
55. R.P. Gangloff, in *Comprehensive Structural Integrity*, eds. I. Milne, R.O. Ritchie, B. Karihaloo (Oxford, U.K.: Pergamon, 2003), p. 31-101.
56. J. Albrecht, I. Bernstein, A. Thompson, *Metall. Trans. A* 13 (1982): p. 811-820.
57. C. Tuck, *Metall. Trans. A* 16 (1985): p. 1503-1514.
58. I. Bernstein, *Mater. Sci. Eng.* 6 (1970): p. 1-19.
59. E.M.K. Hillier, M.J. Robinson, *Corros. Sci.* 46 (2004): p. 715-727.
60. K. Reddy, S. Arumugam, T. Lakshmanan, *J. Mater. Sci.* 27 (1992): p. 5159-5162.
61. L. Duprez, K. Verbeken, M. Verhaege, *Effect of Hydrogen on Materials: Proc. 2008 Int. Hydrogen Conf.*, eds. B. Somerday, P. Sofronis, J. Russell (Materials Park, OH: ASM International, 2008), p. 62-69.
62. C.E. Barth, E.A. Steigerwald, *Metall. Trans.* 1 (1970): p. 3451-3455.
63. H.H. Johnson, J.G. Morlet, A.R. Troiano, *Trans. Metall. Soc. AIME* 212 (1958): p. 528-535.
64. K. Takai, R. Watanuki, *ISIJ Int.* 43 (2003): p. 520-526.
65. G. Scamans, C. Tuck, in *Environment-Sensitive Fracture of Engineering Materials*, ed. Z.A. Foroulis (Englewood, CO: The Metallurgical Society of AIME, 1977), p. 464-483.
66. S.Y. Tsai, H.C. Shih, *J. Electrochem. Soc.* 145 (1998): p. 1968-1976.
67. V. Knotek, V. Hošek, D. Vojtěch, P. Novák, J. Šerák, A. Michalcova, F. Průša, T. Popela, M. Novák, in Proc. 19th Int. Conf. on Metallurgy and Materials (Czech Republic, Rožnov pod Radhoštěm, 2010), p. 1-6.
68. M.A.V. Devanathan, Z. Stachurski, *Proc. R. Soc. London. Ser. A Math. Phys.* 270 (1962): p. 90-102.
69. P. Spatz, H.A. Aebiseher, A. Krozer, L. Schlapback, *Int. J. Res. Phys. Chem. Chem. Phys.* 181 (1993): p. 393-397.
70. A. Atrens, N. Winzer, G. Song, W. Dietzel, C. Blawert, *Adv. Eng. Mater.* 8 (2006): p. 749-751.
71. C. Nishimura, M. Komaki, M. Amano, *J. Alloys Compd.* 293-295 (1999): p. 329-333.
72. H.G. Schimmel, G.J. Kearley, J. Huot, F.M. Mulder, *J. Alloys Compd.* 404-406 (2005): p. 235-237.
73. N.N. Aung, W. Zhou, *Corros. Sci.* 52 (2010): p. 589-594.
74. R.M. Latanision, O.H. Gastine, C.R. Compeau, in *Environment-Sensitive Fracture of Engineering Materials*, ed. Z. Foroulis (Englewood, CO: The Metallurgical Society of AIME, 1977), p. 48-70.
75. G.S. Frankel, A. Samaniego, N. Birbilis, *Corros. Sci.* 70 (2013): p. 104-111.
76. R. Tunold, H. Holtan, M. Berge, A. Lasson, R. Steen-Hansen, *Corros. Sci.* 17 (1977): p. 353-365.
77. H. Vogt, M.O. Speidel, "Effect of Temperature on the Growth Rates of Stress Corrosion Cracks in Metal Alloys Exposed to Water," in CORROSION/96, paper no. 96265 (Houston, TX: NACE International, 1996).
78. J. Renner, H.J. Grabke, *Z. Met.* 69 (1978): p. 639-642.
79. S. Naito, M. Yamamoto, M. Doi, M. Kimura, *J. Electrochem. Soc.* 145 (1998): p. 2471-2475.
80. J. Kearns, *J. Nucl. Mater.* 43 (1972): p. 330-338.
81. S.P. Lynch, *Scr. Metall.* 21 (1987): p. 157-162.